



# Robotic pullback technique of a precurved cochlear-implant electrode array using real-time impedance sensing feedback

Katherine E. Riojas<sup>1</sup> · Trevor L. Bruns<sup>1</sup> · Josephine Granna<sup>1</sup> · Robert J. Webster III<sup>1</sup> · Robert F. Labadie<sup>2</sup>

Received: 26 May 2022 / Accepted: 4 October 2022 / Published online: 4 November 2022  
© CARS 2022

## Abstract

**Purpose** During traditional insertion of cochlear implant (CI) electrode arrays (EAs), surgeons rely on limited tactile feedback and visualization of the EA entering the cochlea to control the insertion. One insertion approach for precurved EAs involves slightly overinserting the EA and then retracting it slightly to achieve closer hugging of the modiolar. In this work, we investigate whether electrical impedance sensing could be a valuable real-time feedback tool to advise this pullback technique.

**Methods** Using a to-scale 3D-printed scala tympani model, a robotic insertion tool, and a custom impedance sensing system, we performed experiments to assess the bipolar insertion impedance profiles for a cochlear CI532/632 precurved EA. Four pairs of contacts from the 22 electrode contacts were chosen based on preliminary testing and monitored in real time to halt the robotic insertion once the closest modiolar position had been achieved but prior to when the angular insertion depth (AID) would be reduced.

**Results** In this setting, the open-loop robotic insertion impedance profiles were very consistent between trials. The exit of each contact from the external stilet of this EA was clearly discernible on the impedance profile. In closed-loop experiments using the pullback technique, the average distance from the electrode contacts to the modiolar was reduced without greatly affecting the AID by using impedance feedback in real time to determine when to stop EA retraction.

**Conclusion** Impedance sensing, and specifically the access resistance component of impedance, could be a valuable real-time feedback tool in the operating room during CI EA insertion. Future work should more thoroughly analyze the effects of more realistic operating room conditions and inter-patient variability on this technique.

**Keywords** Cochlear implants · Impedance sensing · Robotic surgery · Otolaryngology

## Introduction

Cochlear implants (CIs) successfully restore hearing to hundreds of thousands of people worldwide [1]; however, the ultimate success of these implants—hearing quality—is highly correlated with insertion quality. Deeper angular insertion depths (AIDs), smaller distance between electrode array (EA) contacts and the neural endings they are attempting to stimulate (i.e., closer to the inner wall of the cochlea, the modiolar), and minimal trauma have been shown to lead to better audiologic outcomes [2, 3]. Unfortunately, surgeons

typically insert the EA with little visual feedback (i.e., cannot see beyond where the EA enters the cochlea) and limited tactile feedback [4, 5]. Traditional feedback mechanisms commonly used in medical devices and surgical robotics are not applicable to CI EA insertion due to lack of line of sight (ruling out optical tracking) and space constraints/accuracy requirements (precluding magnetic tracking and endoscopy). Imaging feedback tools for analysis of CI placement include preoperative CT scans with customized insertion plans [6], postoperative CT [7], preoperative magnetic resonance imaging to determine candidacy [8], and real-time fluoroscopy during surgery [9]. However, these techniques are burdened by cost, patient radiation exposure, and/or lack of true real-time visualization [10]. Custom EAs have also been designed that incorporate strain gauges [11], scanning electrochemical microscopy [12], or an electromagnetic sensor [13] for position sensing but integrating such sensors into commercial EAs is not currently feasible.

✉ Katherine E. Riojas  
ktriojas@gmail.com

<sup>1</sup> Department of Mechanical Engineering, Vanderbilt University, Nashville, TN, USA

<sup>2</sup> Department of Otolaryngology, Medical University of South Carolina, Charleston, SC, USA

These limitations have led to the search for another source of intraoperative position feedback, ideally one that does not impede workflow, add radiation, increase cost, or involve design of a new EA. In this work, we investigate the use of electrical impedance (hereafter referred to simply as impedance) sensing as one possible tool for insertion feedback. Impedance sensing typically involves sending a biphasic, charge-balanced current pulse to an electrode contact and measuring the voltage response on one or multiple electrode contacts. It has been shown that the impedance values resulting from the electrode–electrolyte interaction can be modeled as an equivalent circuit to gain more specific information from the single measurement [4, 14–21].

Several groups have investigated the use of impedance sensing for proximity detection in cochlear implant surgery. Using a custom EA, Watanabe was one of the first to show the correlation between electrochemical measures and the space between the EA body and the modiolar wall (E-M proximity) [22]. Later experiments [16, 23–25] and simulations [26] reinforced the relationship between impedance and E-M proximity. In particular, Pile et al. demonstrated the correlation between the manufacturer-provided real-time bipolar (1.5 s for 21 pairs) impedance values and the E-M area in phantom and cadaver models using a custom robotic platform for insertion [24]. They showed that impedance values for the precurved EA could be used to distinguish between insertion techniques. Giardina et al. analyzed the relationship between the equivalent circuit model components from [15] and the E-M distance using monopolar stimulation in pseudo-real time with a straight EA in a plastic phantom model [16]. They fit a linear regression model to these measures and found a strong correlation between the access resistance and the E-M distance. Aebischer et al. demonstrated that impedance values could be used after insertion to predict the overall insertion depth of a straight EA without CT scanning [21]. Dong et al. showed that retrospective analysis of the access resistance component of the postoperative impedance could be used to detect translocation without imaging [27]. Additionally, recent work by Klabbers et al. demonstrated that viewing a heatmap of the transimpedance matrix can be more reliable than fluoroscopy imaging to accurately detect tip fold-over after insertion [28]. Finally, Lee et al. have shown that impedance differences can detect when the pullback technique (i.e., pulling a precurved EA back after full insertion to cinch the EA against the modiolar and decrease E-M distance) has been used as opposed to insertion without pullback [29].

A reliable feedback mechanism could prove useful for both manual and robotic control of CIEA insertion. Pile et al. demonstrated using force feedback to detect and react to EA tip fold-over [30]. They then modified the control scheme to use sensed impedance values to adjust precurved EA stylet

actuation [31]. Recently, Hafeez et al. used impedance feedback and machine learning algorithms to gain insight into straight EA positioning in real time and to robotically correct the trajectory of the EA [32]. In a similar way to these works, impedance feedback could be used to aid manual pullback, which is currently performed blindly with limited tactile feedback. This study builds on the aforementioned work by utilizing real-time measurements of the access resistance component of impedance as feedback to modulate a robotic insertion tool to optimize pullback such that the E-M distance is minimized without compromising AID.

## Experiments

To investigate real-time bipolar access resistance insertion profiles for a precurved EA, two experiments were performed using a custom-designed modular testing platform, a robotic insertion tool [33], a digital camera for proximity determination, a custom-printed circuit board (PCB) for impedance sensing [25], and a CI532/632 EA (Cochlear Limited, Sydney, AU). The robotic insertion tool from [33] was slightly modified to enable use with this precurved EA and consists of two piezoelectric linear actuators (SmarAct, Oldenburg, Germany), a 3D-printed housing, slotted tubes for gripping the EA (inner tube) and for grasping the external stylet (outer tube), and a 3D-printed gripper attached to the outer tube for stylet grasping (see Fig. 1b).

In this work, a charge-balanced biphasic current pulse was applied to the stimulating electrode contact, and the corresponding access resistance component of the first-order equivalent circuit model of the electrode–electrolyte interface was analyzed for the immediately adjacent electrode contact as in [25]. This circuit model consists of a resistor in series with a parallel resistor and capacitor. The access resistance represents the DC component of this circuit—the series resistor—and is meant to capture the time-independent impedance components. A current pulse width of 55  $\mu$ s at a pulse magnitude of 100  $\mu$ A was used, and the microcontroller obtained a voltage measurement every 8.5  $\mu$ s during the positive half of the biphasic pulse. To improve effective resolution, if measuring the impedance of 4 pairs of contacts, voltage samples during 20 consecutive pulses were averaged and processed before beginning the cycle again for the next pair for an effective sampling frequency of 60 Hz. When measuring 11 pairs of contacts, only 14 consecutive pulses were averaged together for an effective sampling frequency of 30 Hz.

The phantom model used to mimic a human cochlea was a to-scale model of the scala tympani (ST) chamber of the cochlea with a cochleostomy opening. Cross-sectional dimensions of this model can be viewed in [34]. In this work,

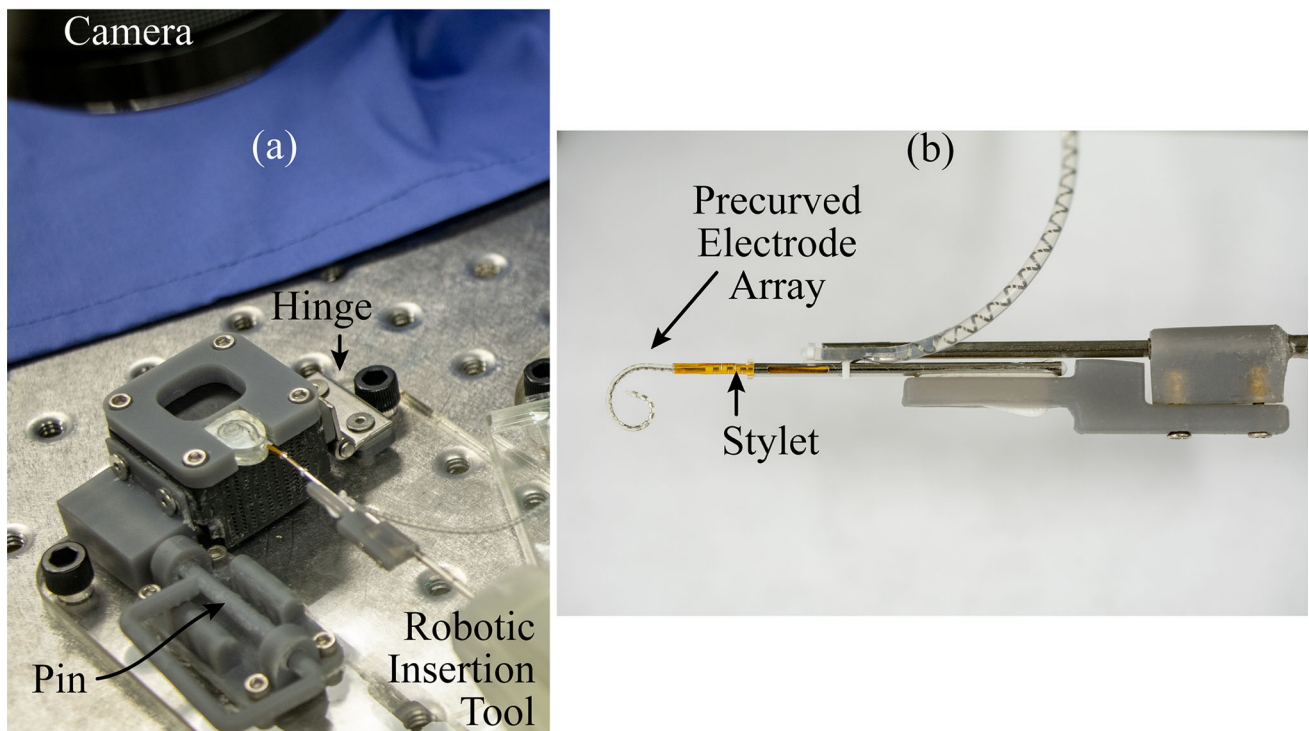


**Fig. 1** **a** Experimental setup for phantom model insertions with the CI532/632 precurved EA and **b** close-up of gripping mechanism

the model was 3D-printed in WaterShed XC material at Protolabs (Maple Plain, MN, USA). A 0.9% saline solution was used to mimic human perilymph since it has been shown to have similar electrical properties to the natural conductive fluid in the ST [35]. The general experimental setup can be seen in Fig. 1.

### Open-loop experiments

In open-loop testing, the general impedance profiles of all available pairs of electrode contacts along the 22-contact precurved EA were evaluated while robotically inserting the EA at 0.38 mm/s into the ST model. This was accomplished in two stages since the current custom impedance sensing PCB was designed to simultaneously measure a maximum of 11 pairs. Thus, ten total trials were performed where the most apical 11 pairs were monitored during the first five trials and the most basal 11 pairs during the second five. For each trial, the EA was inserted and retracted while recording video (30 fps) and access resistances (sampled at 30 Hz). In this experiment, the 0 mm datum was defined as when the EA and external stylet were inserted to the point where the external stylet stopper was at the cochleostomy entrance. In each trial, the EA was inserted from 0 to 11 mm past the inserted stylet, held for 10 s, and then retracted back to 0 mm. A figure showing stages of the open loop experiment insertion and retraction is shown in Fig. 2. Figure 2a shows the EA

tip aligned with the zero-millimeter datum, Fig. 2b shows a snapshot along the insertion, and Fig. 2c shows the EA at full insertion for open-loop experiments. Finally, an image of the EA along its retraction path is shown in Fig. 2d. See the supplementary video for an example of an insertion and retraction in one open-loop experiment trial.

### Closed-loop experiments

After open-loop evaluation was complete, preliminary experiments with the pullback technique were used to select the electrode contact pairs with the highest percent rises in access resistance to pullback for use in closed-loop experiments. Using the same setup as in open-loop experiments but inserting to 14 mm instead of 11 mm past the stylet, the 4 contact pairs with the highest percent rise in access resistance to the first 1.3 mm of pullback out of all 21 pairs were selected for use in closed-loop testing. The goal of this set of experiments was to use the access resistance values to advise when to stop retracting the EA (i.e., to inform when modiolar proximity had been maximized without reduction in AID). A robotic operating system (ROS) architecture was used to stream access resistance data to the linear actuators inside the automated insertion tool.

As before, the EA was inserted under robotic control at 0.38 mm/s. However, during the stationary portion after over-insertion, the resistance of each of the 4 chosen pairs was

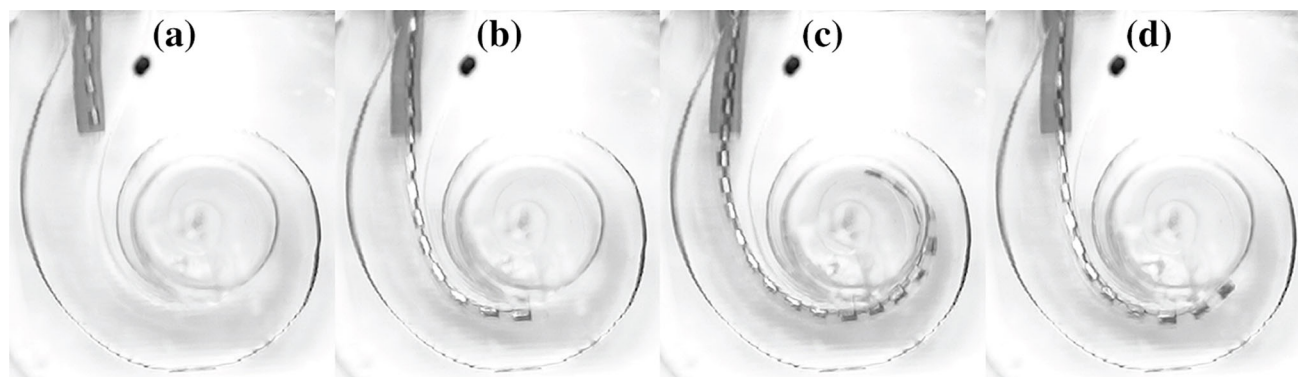


**Fig. 2** Sequence of images showing an open-loop experiment insertion and retraction. **a** EA tip aligned with zero-millimeter datum, **b** snapshot along insertion, **c** full insertion, and **d** snapshot along retraction

recorded. After the ten second hold, retraction began, and the actuators stopped once the resistance of all four pairs had risen by at least the specified percentage above their resting state value. This experiment was repeated for two different over-insertion lengths, 12 mm and 13 mm past the stylet, as well as with two different cutoff percentages, 40% and 60%. Three trials were completed for each configuration, resulting in a total of 12 trials. These test conditions can be viewed in the titles of each of the four plots in Fig. 5. See the supplementary video for an example of a type (iv) trial.

Using an image taken during the ‘at-rest’ portion of the insertion (i.e., once the specified insertion depth had been achieved) and the final retracted position, the average of the distances between the control contacts to their closest points on the modiolus (termed  $\bar{m}$  for the remainder of this paper) and the overall AID were determined. The steps of image analysis can be viewed in Fig. 3. To calculate the change in AID and  $\bar{m}$ , Step 1 was first performed as shown in Fig. 3—adding a filter to the image, and then adding image overlays to increase the ease of image segmentation. These overlays included marking the following locations with circles: the control electrode contacts, the center of the ST, the zero AID location of the ST, the most apical electrode contact, and the extents of the ST. Splines were overlaid on the EA body surrounding the control electrode contacts as well as along the modiolus in the region near the control electrode contacts.

Next, in Step 2, MATLAB (Natick, MA, USA), was used to segment the edited image and calculate the  $\bar{m}$  and AID data. Based on the known color of each overlay, each of these circles and polygons could be extracted in image space. The ST extents were used to generate a scale factor between image pixels and millimeters for each image. The zero AID, center, and tip electrode contact circles were used to generate the AID. The AID was computed as the angle between the zero AID vector and the EA tip vector, shown as the two dashed

green lines in the far-right image of Fig. 3. Finally, localizing the electrode contact positions, EA body, and modiolus enabled computation of the distance between the closest point on the modiolus to the electrode contact and its corresponding closest point on the EA body. These distances are illustrated by the yellow solid lines between the corresponding points for each electrode contact. The  $\bar{m}$  for each image was computed as the average of each of the 5 distances for a given image.

These steps were performed for an image taken before pullback but at full insertion and an image taken after pullback and after the actuators had been turned off based on the resistance readings. Then, we computed the difference in  $\bar{m}$  and AID between the two instances to determine the change in  $\bar{m}$  and AID after pullback.

## Results

### Open-loop experiments

For open-loop testing, the access resistance vs. insertion depth plots for the most apical 11 pairs can be viewed in Fig. 4 (top row) and most basal 11 pairs in Fig. 4 (bottom row). Note that trial 1 of the apical 11 pairs was conducted at a different speed than the rest of the trials and thus was omitted from analysis. Insertion speed should theoretically not affect these results as the authors have seen in preliminary testing, but since this effect has not been rigorously explored, this trial was omitted. It is important to note that the CI532/632 EA features an external stylet—a slotted polyimide tube. This has unique implications when using impedance sensing because it essentially negates the use of the sensing method for proximity detection when the electrode contacts in a sensed pair are enclosed within the stylet tube. Furthermore, due to the slotted openings of the stylet, large fluctuations in sensed impedances occur depending on where the electrode contact

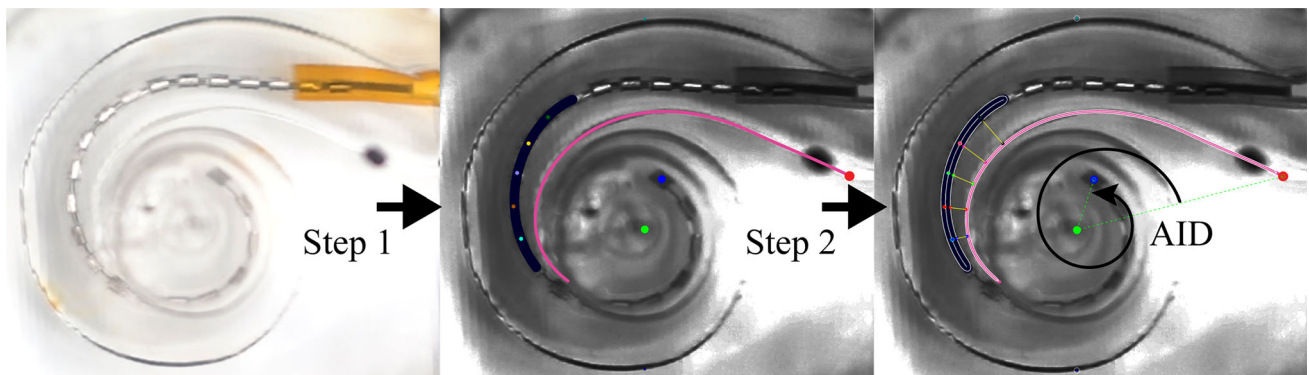


**Fig. 3** Image analysis steps for closed-loop experiment analysis for trial of type (iv). In Step 1, a filter and overlays were added to the image to increase the ease of image segmentation. In Step 2, MATLAB was used to segment the specific locations of the overlays. This enabled computation of the  $\bar{m}$ , defined as the average of the 5 closest point distances

(shown as solid yellow lines in the far-right image). It also enabled computation of AID, the angle between the zero degree and tip electrode contact vector, i.e., angle between the two dashed green vectors shown on the far-right image

is relative to a slot at any given time. These implications demonstrate why the zero point of these experiments was defined as when the stylet was completely inserted into the model (about 5 mm) with the EA tip at the opening of the stylet as described in the “Experiments” section.

Figure 4 shows that the access resistance insertion profile for this setup was very repeatable, and the exit of the electrode contacts from the stylet could be very reliably detected based on the sharp drop in resistance upon exit (in these experiments, a drop of over  $1800 \Omega$  in 1.5 mm of travel). Pairs 17 through 21 (the most basal pairs) did not exit the stylet as can be seen on their plots by their lack of this sharp drop in access resistance. Pair 16 also did not reach this threshold since its more basal electrode contact was still within the stylet even at full insertion.

### Closed-loop experiments

Using results from preliminary testing, the 4 contact pairs with the highest percent rise in access resistance to the first 1.3 mm of pullback were selected for use in closed-loop testing. Assuming the most apical contact is considered contact ‘1,’ second most apical is ‘2,’ and so on, pairs 10–11, 11–12, 12–13, and 13–14 were selected to advise the actuators when to stop the insertion in closed-loop testing. A total of 12 trials were performed, with three trials performed of each trial type. The access resistance vs. time data for all trials is shown in Fig. 5, and trial type specifications can be viewed in the title of each plot. An overview of the difference in  $\bar{m}$  and AID before and after pullback as computed by image analysis is shown in Fig. 6 where the reduction in AID is shown on the horizontal axis and the reduction in  $\bar{m}$  on the vertical axis.

These results demonstrate that for most types of insertion with the specified feedback, the pullback portion successfully increased modiolar hugging (i.e., decreased  $\bar{m}$ ) and did

not substantially affect AID. The 60% rise would clearly not work for a 12 mm insertion since the  $\bar{m}$  before pullback is already quite small, and thus, the tracked electrode contacts essentially must be inside the stylet for the access resistance to rise high enough to meet the cutoff criterion. This result provides an example of what could happen if a surgeon were to pull back too far with limited feedback, and it is clear this erroneous pullback could be viewed if watching the impedance profiles in real time. It also demonstrates the importance of aligning the specification of the overinsertion depth, percent rise criterion, and choice of control electrode contacts to the chosen EA and patient’s ST. A comparison of the final EA positioning for one open-loop trial and one type (iv) closed loop trial is shown in Fig. 7 where the higher insertion depth and similar modiolar-hugging can be visualized.

### Discussion

The real-time access resistance insertion profile for this EA was evaluated for the first time, and open-loop experiments demonstrated that the custom PCB sensing system can be used with a precurved EA. It was evident from this experiment that the external stylet complicates the use of sensing in regions when the electrode contacts of interest are inside the stylet. Even if the external stylet were to be redesigned without the slotted openings, the enclosed nature of the electrode contacts when they are within the stylet would not enable accurate proximity information. The external stylet would need to feature a lengthwise continuous slot that was the width of the electrode contact pads or wider and aligned with the contacts. An internal stylet would of course also solve this challenge.

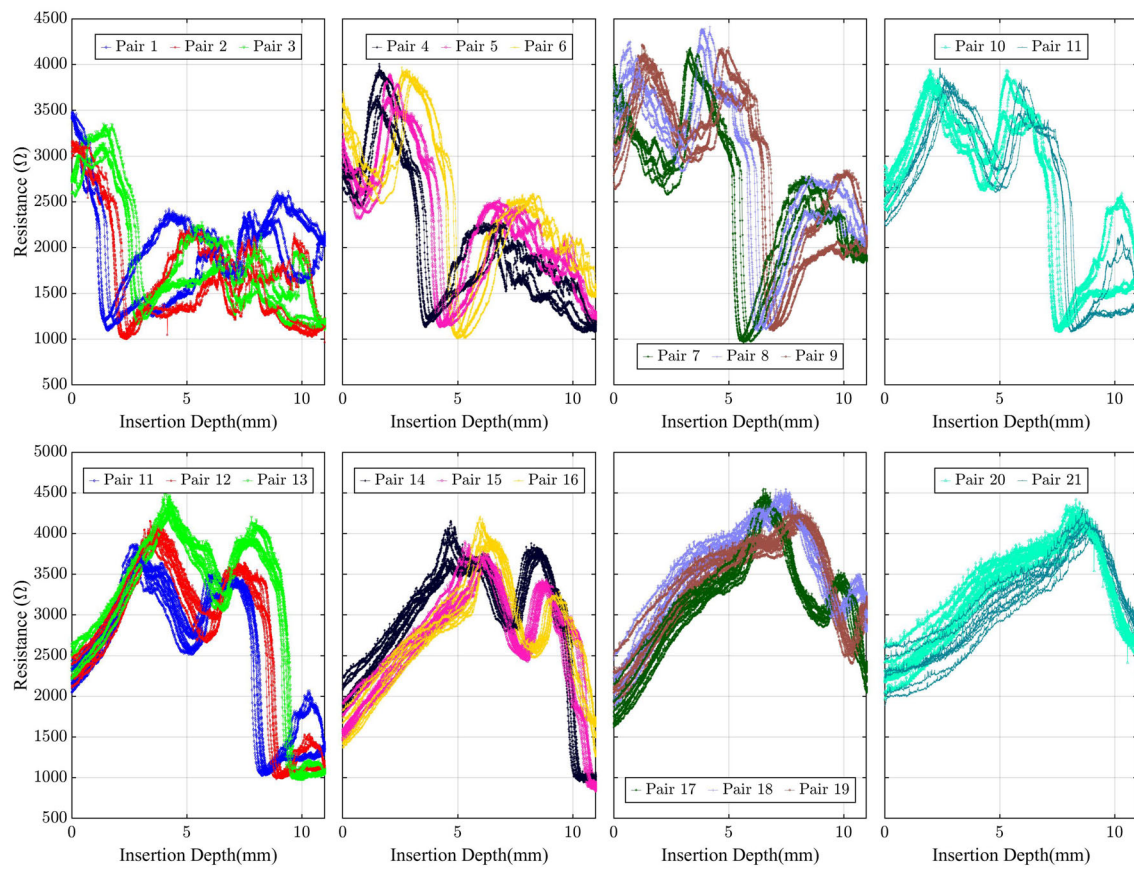


**Fig. 4** Open-loop experiments evaluating the insertion access resistance profile during a normal insertion of the most apical 11 pairs of contacts (top row) and most basal 11 pairs of contacts (bottom row)

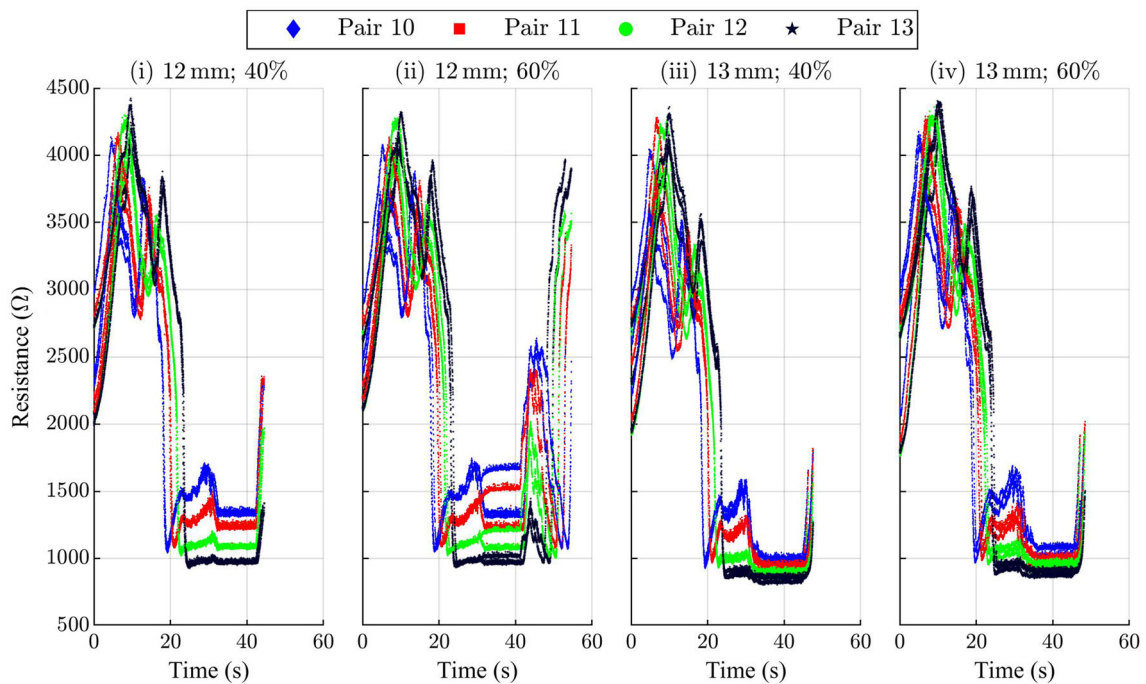


**Fig. 5** Raw access resistance vs. time with the 4 trials overlaid for closed-loop experiment trials of types (i–iv) showing the resistance profile before the linear actuator stop. The insertion depths listed in each subplot title are the distance past the inserted styllet

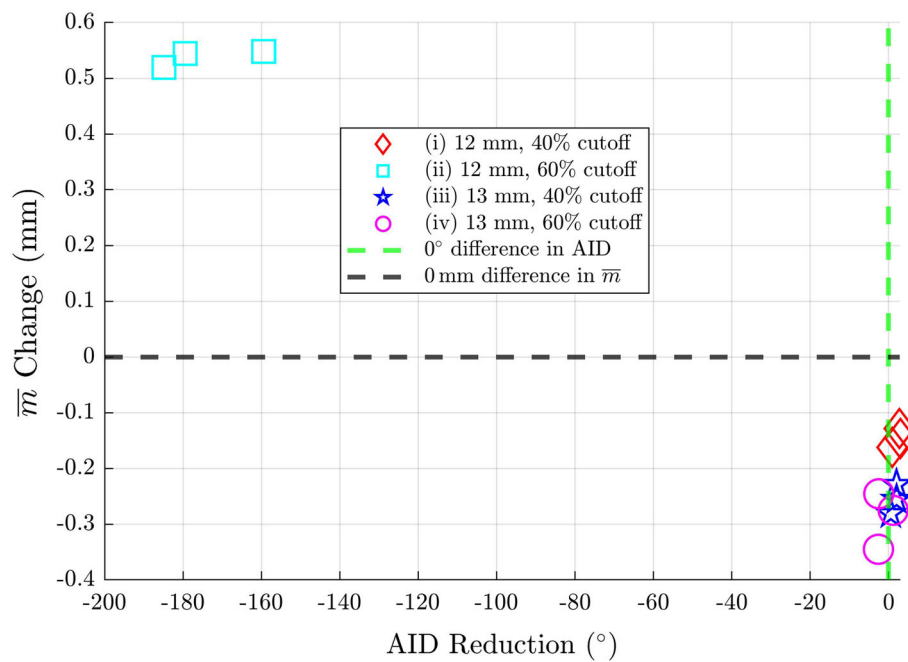


**Fig. 6** Overview of reduction in modiolar distance vs. AID reduction for all trials types (i)–(iv) of closed-loop experiments. On the y-axis, the reduction in average electrode contact-to-modiolus distance ( $\bar{m}$ ) after pullback is shown. Note the desired outcome is for the  $\bar{m}$  to be reduced after pullback. Positive results on the y-axis indicate that upon pullback, the electrode contacts got further from the modiolus. A gray dashed line is shown at 0 mm for ease of viewing those trials that exhibited an increase in  $\bar{m}$ . On the x-axis, the reduction in angular insertion

depth after pullback is shown. Note that the desired outcome is for the AID to remain unchanged after pullback (i.e., a reduction of 0°). A green dashed line is shown at 0° for ease of viewing those trials that had nonzero reductions. These results show that with access resistance feedback and this experimental protocol, most trial types exhibited very little change in AID, but a decrease in the distance to the modiolus as desired

The sensed resistance values of the precurved EA were successfully used in closed-loop experiments to objectively detect when optimal EA positioning had been achieved which could potentially replace subjective tactile feedback. From Fig. 6, it is evident that for most insertion types (see Fig. 5 all but type (ii)), using access resistance feedback to know when to cease pullback resulted in an AID that was relatively unchanged (as desired), with distance to the modiolus,  $\bar{m}$ , reduced as desired. The type (ii) insertion was not hypothesized to work well and is included as an example of poorly performed pullback technique due to limited feedback.

In this work, we utilized a to-scale clear plastic phantom model to enable analysis of the EA positioning in real-time. To prescribe next steps for translation of this work, it should be noted that this phantom model presents key limitations and differences compared to a human cochlea, notably that the walls of the model are not leaky and thus the electrical spread is greatly reduced. By utilizing bipolar impedance sensing between two neighboring electrode contacts, we sought to reduce the effects of anatomical factors on this measurement. Recent work of this bipolar impedance sensing method [36] demonstrated that the power-law relationship between access resistance and E-M proximity in bipolar stimulation holds in

a cadaveric cochlea for this impedance sensing setup, increasing confidence in the translational potential of this work.

Additionally, the artificial perilymph used in these experiments was saline, which has been shown to have similar electrical properties to perilymph [35]; however, further analysis should be done in the future of the nuanced effects that using actual human perilymph can have on these readings.

Finally, future work should investigate how generalized the cutoff conditions and choice of control contacts determined in this study for this average ST model could be. It should be analyzed whether a pre-insertion calibration would be necessary to determine patient-specific cutoff conditions in the future, although the percent rise was purposefully used here to mitigate patient-specific effects. It is likely that the choice of control contacts could be determined simply based on cochlear duct length (using a patient's preoperative CT scan) and their selected EA, but this relationship should be investigated further.

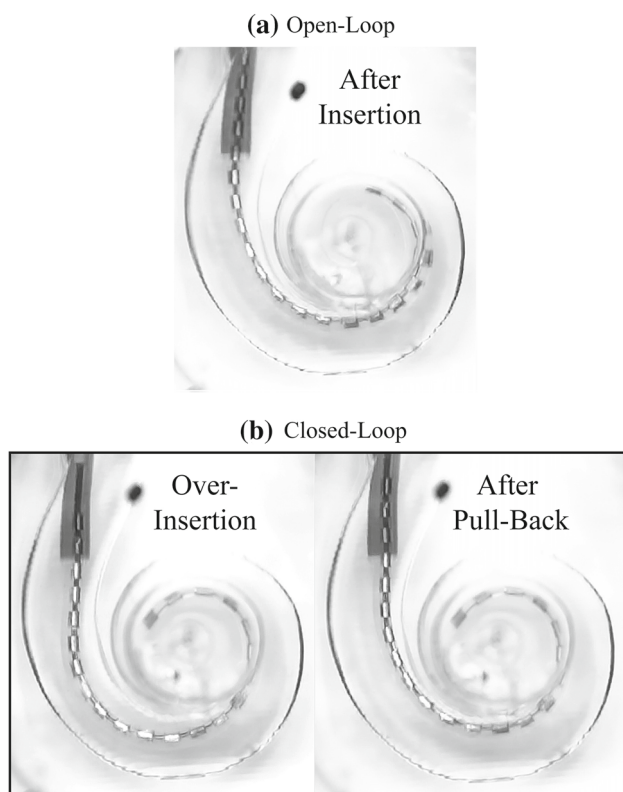


**Fig. 7** **a** Open-loop 11 mm insertion depth final EA positioning vs. **b** closed-loop 13 mm insertion depth (left) before impedance-advised pullback and (right) final EA positioning after pullback. This figure demonstrates deeper insertion depth and similar modiolar-hugging in this closed-loop trial compared with an open-loop trial

## Conclusion

In summary, these data demonstrate that bipolar impedance sensing, specifically the access resistance component of the impedance, has potential for informing EA positioning and improving CI insertions by reducing the average distance between electrode contacts and the modiulus without reducing AID. This modality could provide reliable real-time EA position information without adding extra cost to the surgical procedure nor impeding normal workflow.

**Supplementary Information** The online version contains supplementary material available at <https://doi.org/10.1007/s11548-022-02772-3>.

**Acknowledgements** The authors thank Peter Gibson of Cochlear Ltd. for providing the EAs used in these experiments.

**Funding** This work was supported in part by the National Science Foundation Graduate Research Fellowship under DGE-1445197/1937963.

## Declarations

**Conflict of interest** R.F.L. is a consultant for Advanced Bionics and Medtronic. No other conflicts of interest.

## References

1. What are cochlear implants for hearing? | NIDCD. <https://www.nidcd.nih.gov/health/cochlear-implants>. Accessed 21 July 2020
2. Carlson ML, Driscoll CLWW, Gifford RH, Service GJ, Tombers NM, Hughes-Borst BJ, Neff BA, Beatty CW (2011) Implications of minimizing trauma during conventional cochlear implantation. *Otol Neurotol* 32(6):962–968. <https://doi.org/10.1097/MAO.0b013e3182204526>
3. Chakravorti S, Noble JH, Gifford RH, Dawant BM, O’Connell BP, Wang J, Labadie RF (2019) Further evidence of the relationship between cochlear implant electrode positioning and hearing outcomes. *Otol Neurotol* 40(5):617–624. <https://doi.org/10.1097/MAO.0000000000002204>
4. Vanpoucke FJ, Boermans PPB, Frijns JH (2012) Assessing the placement of a cochlear electrode array by multidimensional scaling. *IEEE Trans Biomed Eng* 59(2):307–310. <https://doi.org/10.1109/TBME.2011.2173198>
5. Kratchman, L. B., Schuster, D., Dietrich, M. S., & Labadie, R. F. (2016). Force perception thresholds in cochlear implantation surgery. *Audiol Neurotol* 21(4):244–249
6. Labadie RF, Noble JH (2018) Preliminary results with image-guided cochlear implant insertion techniques. *Otol Neurotol* 39(7):922–928. <https://doi.org/10.1097/MAO.0000000000001850>
7. Labadie RF, Schefano AD, Holder JT, Dwyer RT, Rivas A, O’malley MR, Noble JH, Dawant BM (2020) Use of intraoperative CT scanning for quality control assessment of cochlear implant electrode array placement. *Acta Otolaryngol* 140(3):206–211. <https://doi.org/10.1080/00016489.2019.1698768>
8. Sweeney AD, Carlson ML, Rivas A, Bennett ML, Haynes DS, Wanna GB (2014) The limitations of computed tomography in adult cochlear implant evaluation. *Am J Otolaryngol* 35(3):396–399. <https://doi.org/10.1016/j.amjoto.2014.03.002>
9. Perazzini C, Puechmaillie M, Saroul N, Plainfossé O, Montrieul L, Bécaud J, Gilain L, Chabrot P, Boyer L, Mom T (2020) Fluoroscopy guided electrode-array insertion for cochlear implantation with straight electrode-arrays: a valuable tool in most cases. *Eur Arch Otorhinolaryngol* 1:3. <https://doi.org/10.1007/s00405-020-06151-z>
10. de Rijk SR, Tam YC, Carlyon RP, Bance ML (2020) Detection of extracochlear electrodes in cochlear implants with electric field imaging/transimpedance measurements. *Ear Hear* 41:1196–1207. <https://doi.org/10.1097/aud.0000000000000837>
11. Wang J, Wise KD (2009) A thin-film cochlear electrode array with integrated position sensing. *J Microelectromech Syst* 18(2):385–395. <https://doi.org/10.1109/JMEMS.2008.2011722>
12. Watanabe H, Velmurugan J, Mirkin MV, Svirsky MA, Lalwani AK, Llinas RR (2014) Scanning electrochemical microscopy as a novel proximity sensor for atraumatic cochlear implant insertion. *IEEE Trans Biomed Eng* 61(6):1822–1832. <https://doi.org/10.1109/TBME.2014.2308058>
13. Scheunemann CWD, Taeger J, Brecht SV, Neun T, Hagen R, Lueth TC, Rak KJ (2022) Concept and first Implementation of an intracochlearly navigated Electrode Array for Cochlear Implantation. In: 2022 44th annual international conference of the IEEE engineering in medicine & biology society (EMBC), pp 2560–2564. <https://doi.org/10.1109/EMBC48229.2022.9871850>
14. Vanpoucke FJ, Zarowski AJ, Peeters SA (2004) Identification of the impedance model of an implanted cochlear prosthesis from intracochlear potential measurements. *IEEE Trans Biomed Eng* 51(12):2174–2183. <https://doi.org/10.1109/TBME.2004.836518>
15. Tykocinski M, Cohen LT, Cowan RS (2005) Measurement and analysis of access resistance and polarization impedance in cochlear implant recipients. *Otol Neurotol* 26(5):948–956. <https://doi.org/10.1097/01.mao.0000185056.99888.f3>



16. Giardina CK, Krause ES, Koka K, Fitzpatrick DC (2018) Impedance measures during in vitro cochlear implantation predict array positioning. *IEEE Trans Biomed Eng* 65(2):327–335. <https://doi.org/10.1109/TBME.2017.2764881>
17. di Lella FA, de Marco D, Fernández F, Parreño M, Boccio CM (2019) In Vivo real-time remote cochlear implant capacitive impedance measurements. *Otol Neurotol* 40:S18–S22. <https://doi.org/10.1097/MAO.0000000000002214>
18. Mesnildrey Q, Macherey O, Herzog P, Venail F (2019) Impedance measures for a better understanding of the electrical stimulation of the inner ear. *J Neural Eng* 16(1):016023. <https://doi.org/10.1088/1741-2552/aaecff>
19. Hou L (2019) The feasibility of a novel sensing system for robotic cochlear electrode array feed for hearing preservation. Brunel University London
20. Hafeez N, Du X, Boulgouris N, Begg P, Irving R, Coulsan C, Tourrel G (2019) Towards unblinding the surgeons: complex electrical impedance for electrode array insertion guidance in cochlear implantation. In: Proceedings of the international symposium on auditory and audiological research, vol 7, pp 39–46. <https://proceedings.isaar.eu/index.php/isaarproc/article/view/2017-06>. Accessed 25 May 2020
21. Aebischer P, Meyer S, Caversaccio M, Wimmer W (2020) Intraoperative impedance-based estimation of cochlear implant electrode array insertion depth. *IEEE Trans Biomed Eng* 68:545–555. <https://doi.org/10.1109/tbme.2020.3006934>
22. Watanabe H (2012) Unconventional neural interface intravascular neural interface and electrochemical endoscopy for cochlear implant. New York University
23. Tan C-T, Svirsky M, Anwar A, Kumar S, Caessens B, Carter P, Treaba C, Roland JT (2013) Real-time measurement of electrode impedance during intracochlear electrode insertion. *Laryngoscope* 123(4):1028–1032. <https://doi.org/10.1002/lary.23714>
24. Pile J, Sweeney AD, Kumar S, Simaan N, Wanna GB (2017) Detection of modiolar proximity through bipolar impedance measurements. *Laryngoscope* 127(6):1413–1419. <https://doi.org/10.1002/lary.26183>
25. Bruns TL, Riojas KE, Labadie RF, Webster RJ (2022) Real-time localization of cochlear-implant electrode arrays using bipolar impedance sensing. *IEEE Trans Biomed Eng* 69(2):718–724. <https://doi.org/10.1109/TBME.2021.3104104>
26. Salkim E (2020) Electrode array position guiding in cochlea based on impedance variation: computational study. *Muş Alparslan Üniversitesi Mühendislik Mimarlık Fakültesi Dergisi* 1(1):64–71
27. Dong Y, Briaire J, Siebrecht M, Stronks H, Frijns J (2021) Detection of translocation of cochlear implant electrode arrays by intracochlear impedance measurements. *Ear Hear* 42:1397–1404
28. Klabbbers ĀTM, Huinck ĀWJ, Mylanus ĀEAM (2021) Comparison between transimpedance matrix (TIM) measurement and x-ray fluoroscopy for intraoperative electrode array tip fold-over detection. *Otol Neurotol* 8:1–7. <https://doi.org/10.1097/MAO.0000000000003290>
29. Lee S-Y, Kim YS, Jo HD, Kim Y, Carandang M, Huh G, Choi BY (2021) Effects of in vivo repositioning of slim modiolar electrodes on electrical thresholds and speech perception. *Sci Rep* 11(1):15135. <https://doi.org/10.1038/s41598-021-94668-6>
30. Pile J, Wanna GB, Simaan N (2014) Force-based flexible path plans for robotic electrode insertion. *IEEE Int Conf Robot Autom* 2014:297–303. <https://doi.org/10.1109/ICRA.2014.6906625>
31. Pile J (2015) Wire-actuated parallel robots for cochlear implantation with in-vivo sensory feedback. PhD Dissertation. Vanderbilt University
32. Hafeez N, Du X, Boulgouris N, Begg P, Irving R, Coulsan C, Tourrel G (2022) Real-time data-driven approach for prediction and correction of electrode array trajectory in cochlear implantation. *Appl Sci* 12(13):6343. <https://doi.org/10.3390/app12136343>
33. Bruns TL, Riojas KE, Ropella DS, Cavilla MS, Petruska AJ, Freeman MH, Labadie RF, Abbott JJ, Webster RJ (2020) Magnetically steered robotic insertion of cochlear-implant electrode arrays: system integration and first-in-cadaver results. *IEEE Robot Autom Lett* 5(2):2240–2247. <https://doi.org/10.1109/LRA.2020.2970978>
34. Leon L, Cavilla MS, Doran MB, Warren FM, Abbott JJ (2014) Scala-tympani phantom with cochleostomy and round-window openings for cochlear-implant insertion experiments. *J Med Devices Trans ASME* 8(4):041010. <https://doi.org/10.1115/1.4027617>
35. Hibbert DB, Weitzner K, Carter P (2001) Voltammetry of platinum in artificial perilymph solution. *J Electrochem Soc* 148(1):E1. <https://doi.org/10.1149/1.1344543>
36. Riojas KE (2021) Making cochlear-implant electrode array insertion less invasive, safer, and more effective through design, magnetic steering, and impedance sensing. Vanderbilt University

**Publisher's Note** Springer Nature remains neutral with regard to jurisdictional claims in published maps and institutional affiliations.

Springer Nature or its licensor (e.g. a society or other partner) holds exclusive rights to this article under a publishing agreement with the author(s) or other rightsholder(s); author self-archiving of the accepted manuscript version of this article is solely governed by the terms of such publishing agreement and applicable law.